RAMAN SPECTROSCOPY OF NANOCRYSTALLINE Li-Ti-O SPINELS AND COMPARATIVE DFT CALCULATIONS ON Ti_yO_z AND $Li_xTi_yO_z$ CLUSTERS

Jakub JIRKOVSKÝ[a1], Kateřina MACOUNOVÁ[a2], Hartmut DIETZ[b1], Waldfried PLIETH[b2], Petr KRTIL[a3,*] and Stanislav ZÁLIŠ[a4,*]

[a] *J. Heyrovský Institute of Physical Chemistry, Academy of Sciences of the Czech Republic, v.v.i., Dolejškova 3, CZ-18223 Prague 8, Czech Republic; e-mail: [1] jakub.jirkovsky@jh-inst.cas.cz, [2] katerina.macounova@jh-inst.cas.cz, [3] petr.krtil@jh-inst.cas.cz, [4] zalis@jh-inst.cas.cz*

[b] *Department of Physical Chemistry and Electrochemistry, Dresden University of Technology, Bergstraße 66b, DE-01062 Dresden, Germany; e-mail: [1] hartmut.dietz@chemie.tu-dresden.de, [2] waldfried.plieth@chemie.tu-dresden.de*

Received November 1, 2006
Accepted January 30, 2007

Dedicated to the memory of Professor Jaroslav Koutecký.

Raman spectra of cubic nanocrystalline insertion hosts in Li-Ti-O system were measured for $Li_{1.1}Ti_{1.9}O_{4-\delta}$ spinels and the corresponding delithiated titanium dioxide material. To interpret the measured data optimized geometries of cubic Ti_yO_z and $Li_xTi_yO_z$ were calculated using the DFT cluster approach for clusters containing up to 23 atoms. The calculated geometries were used to predict the density-of-states (DOS) diagrams and vibrational spectra of the corresponding structures upon harmonic approximation. While the DFT approach reproduces satisfactorily the main structural characteristics of Ti_yO_z clusters, the agreement in the case of $Li_xTi_yO_z$ clusters between calculated and real structures is less satisfactory due to the small cluster size. The band gap energies obtained from DOS diagrams represent overestimates of the actual experimental band gap energies measured on cubic Li-Ti-O oxides. The agreement between calculated and measured band gap energy improves with increasing cluster size. Raman spectra calculated under harmonic approximation from the optimized geometries reproduce all important features of the experimental Raman spectra. The agreement of DFT-calculated and experimental Raman spectra improves with increasing size of the cluster.

Keywords: Li-Ti-O spinels; Nanostructures; Raman spectroscopy; DFT calculations; Vibration analysis; Titanium oxides; Ti clusters.

Spinel oxides of Li-Ti-O structure gained significant importance with respect to potential practical use in secondary Li ion batteries[1–6]. In addition to low strain accompanying the Li insertion process, which is inherently as-

Collect. Czech. Chem. Commun. 2007, Vol. 72, No. 2, pp. 171–184

doi:10.1135/cccc20070171

sociated with the spinel structure, there are several papers reporting an outstanding response of Li-Ti-O spinels to high charge/discharge rates[7] as well as a lowered tendency to undergo the phase transition upon Li insertion[4]. It needs to be noted that such unusual behavior is restricted to nanocrystalline forms of Li-Ti-O spinels and can be associated with unusual distribution of the defects within the structure[8]. This defect distribution affects both the Li insertion mechanism[9], and the electronic structure of the reaction product[8]. The understanding of this unusual behavior, however, cannot be based solely on experimental approach and existing experimental data need to be complemented with computational approach.

The computational chemistry approach has been introduced into the field of Li insertion electrochemistry in 1990's. The first-principles calculations[10–12] were successfully used to predict different features of Li insertion hosts like, e.g., phase stability[13,14] or transport properties. In their majority these calculations use either the linearized augmented planar wave (LAPW) or pseudopotential-based methods to predict, e.g., most likely positions of inserted/extracted cations[15], relative stability of different conceivable structures[16] or transport properties of the insertion hosts[12]. In the case of Li-Ti-O ternary system the ab initio calculations were used to resolve the electronic structure of the $Li_4Ti_5O_{12}$ spinel[17,18] and to model X-ray absorption spectra.

The conventional computational approach based on LAPW applied under the periodical boundary condition (i.e. assumption of a semi-infinite crystal) is rather inconvenient in the characterization of the nanocrystalline hosts. An alternative approach is DFT-based calculations when the nanocrystals are approximated by small atomic clusters of finite size[19]. Theoretical investigation of nanostructered materials suffers from several problems such as the convergence problem[20] or surface termination in clusters[21].

The DFT-based cluster calculations in the Li-Ti-O system have been so far focused on optimization of the geometry of small Ti_yO_z clusters constructed either on molecular level or assuming a solid-state structure with tetragonal symmetry[22,23]. The Ti_yO_z clusters derived from rutile structure were optimized for the size of containing up to 3 Ti atoms[24]. In the case of anatase-related clusters, a successful optimization was achieved for a cluster containing up to 16 Ti atoms[21]. The optimized structures were used mainly to construct the density-of-states diagrams, they were not used, except for $(TiO_2)_n$ (n up to 3) clusters, in vibrational analysis[24]. This paper extends the previously done theoretical work on systems related to active insertion phases in the Li-Ti-O system with cubic symmetry – Li-Ti-O spinels and corresponding delithiated cubic TiO_2. The density-of-states obtained on optimized cluster structure are used for theoretical prediction of electronic

spectra of the materials; vibrational analysis of calculated clusters was used to predict the Raman spectra of the optimized clusters. The results of the DFT calculations were used for interpretation of actual experimental spectra.

EXPERIMENTAL

Calculations

Ground state electronic structure calculations on Ti_yO_z and $Li_xTi_yO_z$ clusters have been done by the density-functional theory (DFT) method using Gaussian 03 program package[25]. A valence double-ζ basis with polarization functions, 6-31G*[26], were used for Li, O, Ti and H atoms within Gaussian 03. The comparative calculations were done with the basis using effective quasi-relativistic core pseudopotentials and a corresponding optimized set of basis functions for Ti atoms[27]. Either the "pure" density functional BPW91[28,29], or hybrid Becke's three-parameter functional with Lee, Yang and Parr correlation functional (B3LYP)[30] were used. Geometry optimization of all systems was performed without symmetry constraints; the vibrational analyses were done on optimized structures. The approximate D_{3d} symmetry was used for assignment of Raman spectra of the Ti_7O_{14} cluster. The simulation of Raman spectra was based on calculated Raman intensities.

Chemicals and Measurement

The nanocrystalline cubic Li-Ti-O spinel was prepared by solvothermal synthesis from TiO_2 (P25, Degussa) and LiOH (Aldrich, p.a.) at 200 °C in ethanol. Details of the synthetic procedure can be found elsewhere[31]. The corresponding cubic form of TiO_2 was prepared from the original spinel by extraction in 10 wt.% acetic acid solution at 80 °C for 4 h. All chemicals used in materials preparation were used as received. The structure of the prepared materials was determined by Rietveld analysis of powder X-ray diffraction data gathered using a Bruker Advance 8 diffractometer with CuKα radiation (λ = 1.5418 Å). The Raman spectra were measured using a Renishaw 2000 scan table equipped with Leica microscope. The wavelength of the excitation radiation (He-Ne laser) was 633 nm, the output power of the excitation laser was 17 mW. The final spectra represent typically an average of 12 consecutive scans.

RESULTS AND DISCUSSION

Cluster Geometry Optimization

To test the sensitivity of the DFT cluster approach to the initial structure, we calculated optimized geometry on clusters of comparable size with those reported in refs[22,23] assuming basically cubic arrangement of the clusters. The results of our geometry optimization calculations are summarized in Table I in refs[22,23]. As follows from the data listed in Table I, the initial structure, which is subject to optimization, has a negligible effect on the

optimized cluster geometry until the number of atoms in the cluster does not exceed 8. Under such conditions the cluster behavior approximates that of a molecule and bears limited relevance to the structure imposed on it in real nanocrystalline systems. For bigger clusters containing 9 or 10 atoms, the calculated bond lengths and angles start to reflect the different symmetry of Ti and O in the starting structures. The difference in the observed behavioris is not, however, a dramatic one. Such a tendency can be explained keeping in mind that the symmetry of the Ti as well O in both approaches (i.e. in both starting structure models) is quite similar. The tetragonal approach adopted in refs[22,23] operates with the assumption D'_{2h} and C'_{2v} symmetry of the Ti and O in the starting structure, respectively. This symmetry changes to D_{3d} and C_{3v} in the cubic approach.

The computational approach presented in refs[22,23] needs to be modified if a convergent solution of the DFT calculation is sought for bigger clusters. Utilizing the cubic Ti_4O_8 subunit, we succeeded in obtaining structure optimization on clusters as big as Ti_7O_{14}. In order to avoid the convergence problems, a process involving two iterations was employed for clusters with more than 4 Ti atoms. In the first iteration the free valences were saturated with H atoms. The Ti and O coordinates obtained in the optimization with saturated free bonds were used as the input in the second iteration process leading to optimized geometry of the final structure. Figure 1 depicts the DFT-optimized structures of the clusters containing four and seven Ti atoms. As show the results of the structure optimization summarized in Table I,

TABLE I
Comparison of DFT-calculated bond lengths (in Å) for Ti_4O_8 and Ti_7O_{14} clusters with the crystal structure of cubic TiO_2

Bond	Ti_4O_8	Ti_7O_{14}	Experiment
Ti_2–Ti_1	2.849	2.945	2.970
Ti_2–Ti_2	2.849	2.954	2.970
Ti_2–Ti_2'	–	5.122	5.145
Ti–O	1.999	2.015	2.000
O–O	2.754	2.715	2.671
O–O′	–	6.832	6.513

comparing the calculated characteristic bond lengths with experimental ones, the optimized geometry represents a realistic approach to the cubic TiO_2 structure one may encounter in real nanocrystalline materials. The bond lengths and angles obtained in cluster calculations clearly show sensitivity to cluster size. While the characteristic features of the crystal structure are well reproduced on clusters containing 7 Ti atoms (Ti–Ti and Ti–O distances are reproduced within 0.02 Å), a less satisfactory agreement is recorded for Ti_4O_8 clusters. It should be noted that the theoretically predicted O–O bond lengths deviate from experimental values; the deviation, however, decreases with increasing cluster size.

An application of the DFT cluster approach, used to optimize the geometry of Li-Ti-O spinels, is a more complex task than in the case of cubic titania. The incorporation of lithium cations changes the total charge of the cluster and results in more or less symmetric distortion of the TiO_x framework. The simplest cluster that can be considered as relevant to real spinel nanocrystals corresponds to chemical composition of $Li_2Ti_7O_{14}^{2+}$. Assuming that the TiO_x framework is not dramatically changed by incorporation of Li, there are in principle two arrangements placing the Li ions either sym-

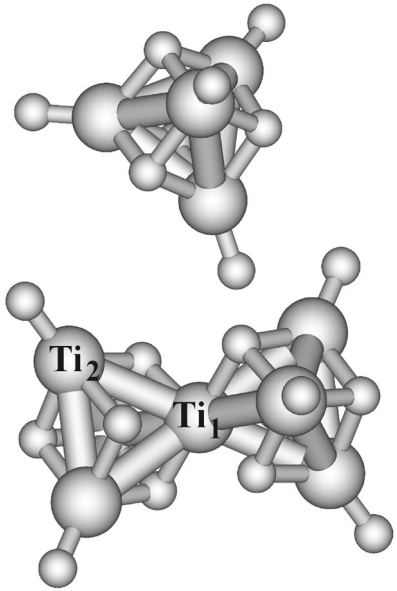

FIG. 1
The DFT-optimized geometry of Ti_4O_8 (top) and Ti_7O_{14} (bottom) clusters

metrically or asymmetrically with respect to the threefold axis of TiO_4 tetrahedra of Ti_7O_{14}. Out of these two arrangements only the symmetric cluster gives a convergent geometry which is shown in Fig. 2. It should be noted that, due to the non-zero charge and relatively small size of the cluster, the optimized geometry is less symmetric than that of corresponding Ti_7O_{14}. The symmetry of the cluster changes from approximately D_{3d} (Ti_7O_{14}) to approximately C_i. As can be expected, the calculated bond lengths fail to reproduce correctly those observed experimentally in real nanocrystals. The incorporated Li has the biggest effect on the Ti–Ti bond lengths where the difference between calculated and measured bond lengths ranges between 0.1 and 0.06 Å. In the case of O–O and Ti–O bond lengths, the calculated model reproduces the experimental values with an accuracy better than 0.05 Å.

Electronic Structures of Optimized Clusters

The density of states (DOS) for systems Ti_4O_8, Ti_7O_{14} and $Ti_7O_{14}Li_2^{2+}$ are plotted in Figs 3 and 4. Both figures show large contribution of Ti orbitals to the lowest-lying unoccupied molecular orbitals (LUMO) and of O orbitals to the highest occupied ones (HOMO). Figure 3 indicates the grouping of orbital levels going from Ti_4O_8 to Ti_7O_{14} and the diminishing HOMO-LUMO separation with growing size of the cluster. The calculated HOMO-LUMO gaps are 5.50, 4.39 and 4.07 eV for Ti_3O_7, Ti_4O_8 and Ti_7O_{14}, respectively. This trend must be expected, corresponding with the well-

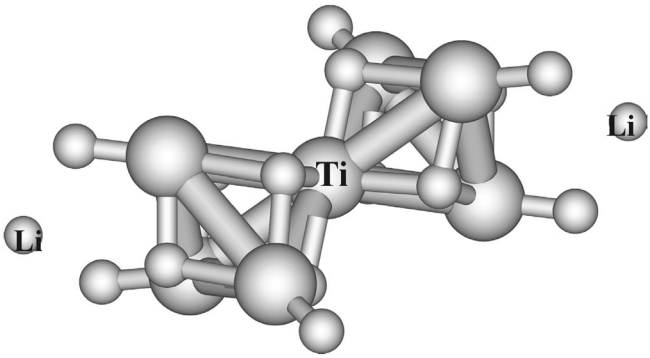

FIG. 2
The DFT-optimized geometry of $Ti_7O_{14}Li_2^{2+}$ cluster

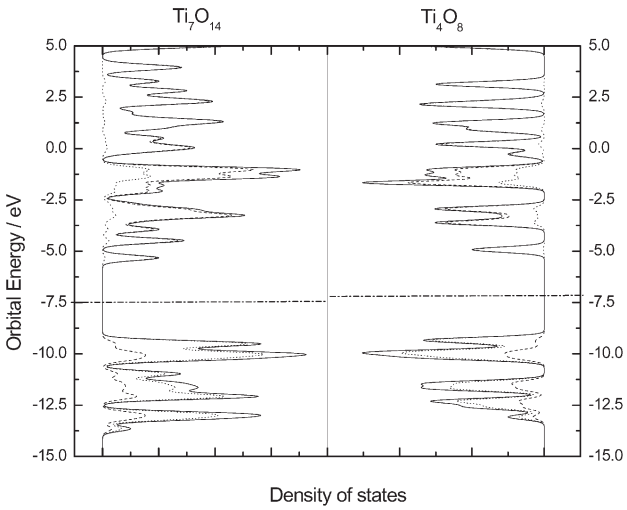

FIG. 3
The B3LYP-calculated density of states for Ti_7O_{14} and Ti_4O_8. Full line indicates total density of states, dashed one contribution from Ti and dotted one from O. Vertical dashed line indicates an approximate midpoint of HOMO-LUMO levels

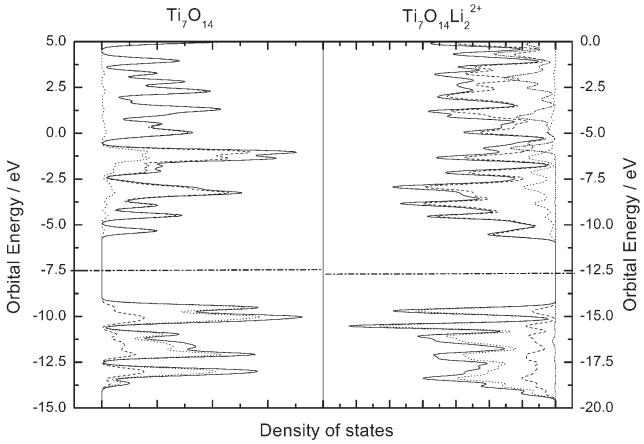

FIG. 4
The B3LYP-calculated density of states for Ti_7O_{14} and $Ti_7O_{14}Li_2^{2+}$. Full line indicates total density of states, dashed one contribution from Ti and dotted one from O. Vertical dashed line indicates an approximate midpoint of HOMO-LUMO levels

known shift of the band gap energy of semiconductors due to the quantum confinement. It should be noted that the calculated values of HOMO-LUMO separations are significantly higher than those reported for tetragonal polymorphs of titania (3.05 and 3.2 eV for rutile and anatase, respectively); the agreement with Li-Ti-O spinel (3.8 eV) is slightly better[8].

A comparison of the calculated electronic structures of Ti_7O_{14} and $Ti_7O_{14}Li_2^{2+}$ is shown in Fig. 4. Analyzing the shape of the DOS diagrams plotted in Fig. 4 one finds that the Li^+ present in the structure has just a small effect on the structure of the occupied (bonding) orbitals and the calculated HOMO-LUMO gap remains practically unchanged. Keeping in mind the small size of the optimized cluster, we may take the calculated HOMO-LUMO separation as a reasonable estimate of the actual band gap of cubic spinels (3.8 eV)[8]. Although the HOMO-LUMO separation of the Li-containing clusters is practically unaffected by incorporation of Li, the actual position of the orbitals on the energetic scale shifts to more negative energy values. This trend can be attributed to the fact that, in contrast to Ti_7O_{14}, the Li containing cluster is a dication.

Raman Spectra and DFT Calculations

An additional test of the relevance of DFT-calculated cluster structures to real nanocrystals is a comparison of the Raman spectra obtained by vibrational analysis of the optimized cluster geometries with experimentally measured Raman spectra. The DFT-calculated Raman-active vibrations for Ti_3O_7, Ti_4O_8 and Ti_7O_{14} model clusters along with experimental Raman bands of the TiO_2 nanocrystals are summarized in Table II. The DFT-predicted Raman-active vibration transitions appear in five regions: 210–250 cm^{-1}, 300–350 cm^{-1}, around 400 cm^{-1}, around 550 cm^{-1} and 610–620 cm^{-1}. The actual position of calculated vibration modes depends on the cluster size and on the symmetry of the given vibration. Assuming that the Raman spectrum of the Ti_7O_{14} cluster bears the closest resemblance to the actual Raman spectra of the real nanocrystals we can say that the calculated totally symmetrical vibrations around 300 cm^{-1} are systematically shifted to higher energies with respect to the experimental transitions. The vibrations of an E_g symmetry show much weaker dependence on the cluster size. This trend can be used to explain less satisfactory agreement of the spectrum simulated for Ti_7O_{14} cluster with that of the nanocrystalline cubic TiO_2 in the spectral regions corresponding to A_{1g} vibrations (Fig. 5). Nevertheless, as can be shown for the vibration giving the worst agreement with

experimental spectra (the totally symmetrical vibration depicted for Ti_4O_8 in Fig. 6), the frequencies of the A_{1g} vibrations shift in the correct direction (i.e. towards values suggested by experiment) going from Ti_3O_7 to Ti_7O_{14}. It must be stressed that no calculated (and observed) Raman-active vibrations correspond to simple vibrations, but to combinations of Ti–O, Ti–Ti, O–Ti–O and Ti–Ti–O stretching and bending modes (see Fig. 6).

A similar procedure was applied to the vibration spectra simulated for the Li-containing cluster $Ti_7O_{14}Li_2^{2+}$ (see Fig. 2 for the optimized structure). The results of comparison of the DFT-predicted spectrum of $Ti_7O_{14}Li_2^{2+}$ and of

TABLE II
DFT-calculated Raman-active frequencies for clusters Ti_3O_7, Ti_4O_8 and Ti_7O_{14}

Calculated ν, cm^{-1}			Experiment ν, cm^{-1}
Ti_3O_7	Ti_4O_8	Ti_7O_{14}	
216.9 (4.9)	246.0 (4.6)	219.7 (7.2)	197
217.0 (4.9)		219.8 (7.3)	
	246.8 (4.5)	257.2 (4.4)	
	247.6 (4.6)	257.5 (4.5)	
	288.5 (2.0)		
289.0 (2.5)	289.7 (2.0)		
349.3 (17.8)	331.2 (18.1)	307.5 (32.4) [A_{1g}]	248
		323.8 (7.2)	
		324.4 (7.0)	
409.5 (4.8)	393.0 (11.3)	402.9 (22.4) [E_g]	411
412.2 (4.8)	394.6 (11.1)	403.6 (21.9) [E_g]	
583.0 (3.7)		556.2 (7.1) [E_g]	551
	565.2 (12.3)	568.7 (9.3) [E_g]	
627.2 (3.5)		606.8 (2.3) [A_{1g}]	602

[a] Raman intensities in parentheses, approximate symmetries in brackets.

the nanocrystalline Li-Ti-O spinel are summarized in Table III and Fig. 7. As follows from Fig. 7, the Raman spectrum predicted by the DFT approach using a relatively small cluster gives a rather satisfactory agreement with experiment. The calculated spectrum reproduces the main features of the experimental spectrum – mainly the spectral regions between 200–300 cm^{-1}

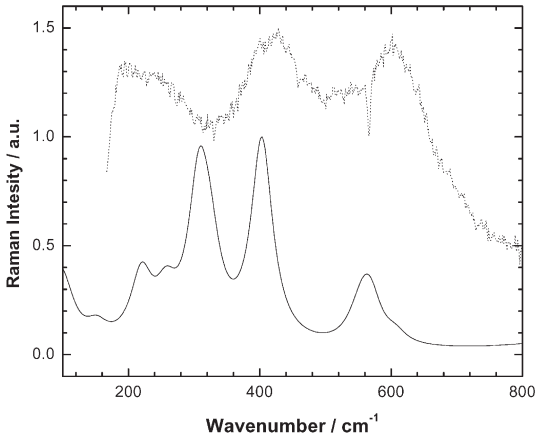

FIG. 5
The experimental Raman spectrum of cubic TiO_2 (dotted line) and calculated spectrum for Ti_7O_{14} cluster (full line)

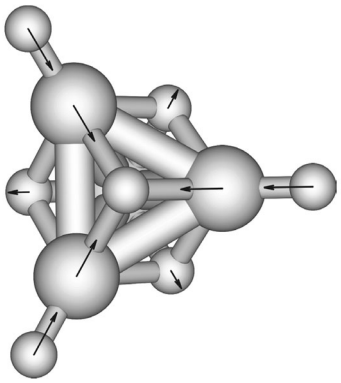

FIG. 6
The schematic representation of the Raman-allowed totally symmetrical representation calculated for Ti_4O_8 (331.2 cm^{-1})

TABLE III

Comparison of selected DFT-calculated Raman-active vibrations for $Ti_7O_{14}Li_2^{2+}$ cluster with the experimental Raman spectrum of Li-Ti-O spinel

Calculated ν, cm^{-1}	Experimental ν, cm^{-1}	Calculated ν, cm^{-1}	Experimental ν, cm^{-1}
227.3 (6.9)		417.8 (7.6)	438
245.4 (11.1)	236	437.0 (4.6)	
248.2 (4.9)		490.1 (10.2)	
257.5 (6.1)		596.7 (17.4)	607
353.3 (4.6)	345	624.7 (7.5)	
368.9 (15.7)		644.3 (11.0)	668
404.7 (32.3)			

[a] Raman intensities in parentheses.

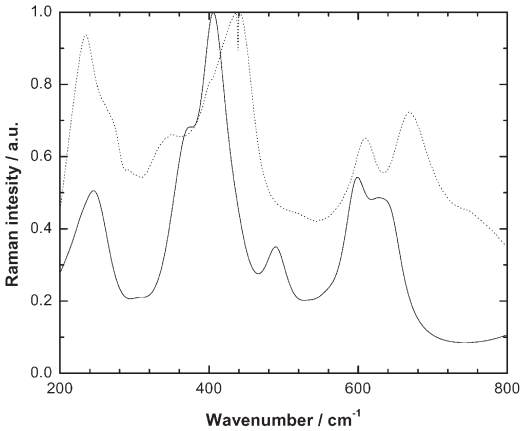

FIG. 7

The experimental Raman spectrum of cubic Li-Ti-O (dotted line) and simulated spectrum for $Ti_7O_{14}Li_2^{2+}$ cluster (full line)

and around 600 cm^{-1}. The experimentally observed vibrations near 440 and 670 cm^{-1} are reproduced less satisfactorily by the calculated spectrum. In both cases the theoretical approach predicts a slightly lower frequency of the vibration by ca. 40 cm^{-1}. Despite this discrepancy, which is most likely associated with the finite size of the DFT-optimized cluster, the DFT approach is capable of predicting the Raman spectra of Li-Ti-O spinel with an acceptable accuracy. The model, however, needs to be enlarged if one considers this approach for the prediction of Raman spectra of partially/fully reduced Li-Ti-O spinels.

CONCLUSIONS

The DFT-based optimization of medium-size clusters followed by vibrational analysis was used in an attempt to predict properties of nanocrystalline cubic TiO_2 and Li-Ti-O spinels. The geometries of clusters of composition Ti_3O_7, Ti_4O_8, Ti_7O_{14} and $Li_2Ti_7O_{14}^{2+}$ were optimized and compared with real crystallographic data of corresponding nanocrystalline phases. The optimized geometry begins to reflect the imposed cubic structure starting from the cluster size of at least 10 atoms. The electronic structures of the optimized clusters indicate broader separation of the HOMO-LUMO levels (which approximates the band gap energy of real nanocrystals) than the one accessible experimentally. Such a behavior must be expected due to the q-size effects connected with their small size. The vibrational analyses of optimized geometries were used to predict the Raman spectra of the above mentioned clusters. Two types of vibrations were found in calculated Raman spectra of the optimized clusters. The totally symmetric vibrations shift towards lower frequencies with increasing cluster size. The dependence of the vibrations with E_g symmetry on the cluster size is much weaker. The overall agreement of the cubic titania-based clusters with the experimentally obtained spectrum is acceptable and can be used for qualitative interpretation of spectral features. The Raman spectra predicted by the DFT approach for the $Ti_7O_{14}Li_2^{2+}$ cluster adequately reflect the main spectral changes induced by Li incorporation. A better quantitative agreement with experiment as well as the possibility to study partially/fully reduced Li-Ti-O spinels, however, requires extension of the system size.

This work has been supported by the Grant Agency of the Academy of Sciences of the Czech Republic (grant No. ET400400413). J. Jirkovský, H. Dietz and W. Plieth highly appreciate financial help from the Deutsche Forschungsgemeinschaft under contract No. 436 TSE 113/43.

REFERENCES

1. Ariyoshi K., Yamamoto R., Ohzuku T.: *Electrochim. Acta* **2005**, *51*, 1125.
2. Arico A. S., Bruce P., Scrosati B., Tarascon J. M., Van Schalkwijk W.: *Nat. Mater.* **2005**, *4*, 366.
3. Persson P., Bergström R., Ojamäe L., Lunell S.: *Adv. Quantum Chem.* **2002**, *41*, 203.
4. Fattakhova D., Krtil P.: *J. Electrochem. Soc.* **2002**, *149*, A1224.
5. Peramunage D., Abraham K. M.: *J. Electrochem. Soc.* **1998**, *145*, 2609.
6. Ohzuku T., Ueda A., Yamamoto N.: *J. Electrochem. Soc.* **1995**, *142*, 1431.
7. Kavan L., Grätzel M.: *Electrochem. Solid State Lett.* **2002**, A39.
8. Kostlánová T., Dědeček J., Krtil P.: *Electrochim. Acta* **2007**, *52*, 1847.
9. Krtil P., Dědeček J., Kostlánová T., Brus J.: *Electrochem. Solid State Lett.* **2004**, *7*, A163.
10. Van der Ven A., Ceder G.: *Phys. Rev. B* **1999**, *59*, 742.
11. Ceder G., Chiang Y. M., Sadoway D. R., Aydinol M. K., Jang Y. I., Huang B.: *Nature* **1998**, *392*, 694.
12. Aydinol M. K., Kohan A. F., Ceder G., Cho K., Joannopoulos J.: *Phys. Rev. B* **1997**, *56*, 1354.
13. Han B. C., Van der Ven A., Morgan D., Ceder G.: *Electrochim. Acta* **2004**, *49*, 4691.
14. McHale J. M., Auroux A., Perrotta A. J., Navrotsky A.: *Science* **1997**, *277*, 788.
15. Benco L., Barras J.-L., Daul C. A., Deiss E.: *Inorg. Chem.* **1999**, *38*, 20.
16. Mishra S. K., Ceder G.: *Phys. Rev. B* **1999**, *59*, 6120.
17. Aldon L., Kubiak P., Womes M., Jumas J. C., Olivier-Fourcade J., Tirado J. L., Corredor J. I., Pérez Vincente C.: *Chem. Mater.* **2004**, *16*, 5721.
18. Lippens P. E., Womes M., Kubiak P., Jumas J. C., Olivier-Fourcade J.: *State Sci.* **2004**, *6*, 161.
19. Ammundsen B., Burns G. R., Saiful Islam M., Kanoh H., Rozière J.: *J. Phys. Chem. B* **1999**, *103*, 5175.
20. Persson P., Gebhardt J. C. M., Lunell S.: *J. Chem. Phys. B* **2003**, *107*, 3336.
21. Noguera C.: *Surf. Rev. Lett.* **2001**, *8*, 121.
22. Albaret T., Finocchi F., Noguera C.: *Faraday Discuss.* **1999**, *114*, 285.
23. Albaret T., Finocchi F., Noguera C.: *Appl. Surf. Sci.* **1999**, *144–145*, 672.
24. Hagfeldt A., Bergström R., Siegbahn H., Lunell S.: *J. Phys. Chem.* **1993**, *97*, 12725.
25. Frisch M. J., Trucks G. W., Schlegel H. B., Scuseria G. E., Robb M. A., Cheeseman J. R., Montgomery J. A., Vreven T., Jr., Kudin K. N., Burant J. C., Millam J. M., Iyengar S. S., Tomasi J., Barone V., Mennucci B., Cossi M., Scalmani G., Rega N., Petersson G. A., Nakatsuji H., Hada M., Ehara M., Toyota K., Fukuda R., Hasegawa J., Ishida M., Nakajima T., Honda Y., Kitao O., Nakai H., Klene M., Li X., Knox J. E., Hratchian H. P., Cross J. B., Adamo C., Jaramillo J., Gomperts R., Stratmann R. E., Yazyev O., Austin A. J., Cammi R., Pomelli C., Ochterski J. W., Ayala P. Y., Morokuma K., Voth G. A., Salvador P., Dannenberg J. J., Zakrzewski V. G., Dapprich S., Daniels A. D., Strain M. C., Farkas O., Malick D. K., Rabuck A. D., Raghavachari K., Foresman J. B., Ortiz J. V., Cui Q., Baboul A. G., Clifford S., Cioslowski J., Stefanov B. B., Liu G., Liashenko A., Piskorz P., Komaromi I., Martin R. L., Fox D. J., Keith T., Al-Laham M. A., Peng C. Y., Nanayakkara A., Challacombe M., Gill P. M. W., Johnson B., Chen W., Wong M. W., Gonzalez C., Pople J. A.: *Gaussian 03*, Revision B.2. Gaussian, Inc., Pittsburgh (PA) 2003.
26. Francl M. M., Pietro W. J., Hehre W. J., Binkley J. S., DeFrees D. J., Pople J. A., Gordon M. S.: *J. Chem. Phys.* **1982**, *77*, 3654.

27. Andrae D., Haeussermann U., Dolg M., Stoll H., Preuss H.: *Theor. Chim. Acta* **1990**, *77*, 123.
28. Becke A. D.: *Phys. Rev. A* **1988**, *38*, 3098.
29. Perdew J. P., Wang Y.: *Phys. Rev. B* **1992**, *45*, 13244.
30. Becke A. D.: *J. Chem. Phys.* **1993**, *98*, 5648.
31. Fatakhova D., Petrykin V. Brus J. Dědeček J., Krtil P.: *Solid State Ionics* **2005**, *176*, 1877.